

## Hydrothermal Synthesis and Electrochemical Properties of N-doped Activated Carbon Microspheres

Tingnan Yan<sup>1,2,†</sup>, Jingli Xu<sup>1,2,†</sup>, Zengyong Chu<sup>2,\*</sup>, Enhui Liu<sup>1,\*</sup>, Luo Yang<sup>1,\*</sup>, Chunhua Wang<sup>2</sup>

<sup>1</sup> College of Chemistry, Xiangtan University, Xiangtan 411105, P.R. China

<sup>2</sup> College of Science, National University of Defense Technology, Changsha 410073, P.R. China

\*E-mail: [chuzy@nudt.edu.cn](mailto:chuzy@nudt.edu.cn), [liuenhui99@sina.com.cn](mailto:liuenhui99@sina.com.cn), [yangluo@xtu.edu.cn](mailto:yangluo@xtu.edu.cn)

Received: 26 March 2017 / Accepted: 25 April 2017 / Published: 12 June 2017

N-doped carbon microspheres were fabricated from glucose using g-C<sub>3</sub>N<sub>4</sub> quantum dots as the nitrogen source under hydrothermal conditions. The carbon microspheres were found remarkably enlarged from 0.4 μm to 5.0 μm after the addition of the quantum dots. Adjustable nitrogen content in the form of pyridinic (N-6) or pyrrolic or pyridone (N-5) was introduced into the carbon microspheres up to 6.48 %. The surface areas of the activated carbon microspheres are comparable to those of the un-doped smaller ones. Electrochemical analysis indicates that nitrogen doping leads to both enhanced conductivity and enhanced specific capacitance up to 281 F/g at 2 A/g.

**Keywords:** activated carbon microspheres, hydrothermal synthesis, glucose, g-C<sub>3</sub>N<sub>4</sub>, specific capacitance.

### 1. INTRODUCTION

Carbon materials are widely used for electric double layer capacitors. Kalpana [1] used waste papers as raw materials to fabricate activated carbon-based super capacitors for the first time. Kierzek [2] prepared carbon electrodes with the bituminous coal and mesophase pitch. Bananas were also used as the carbon precursor to fabricate the multilevel microstructures with high specific capacitance and good cyclic performance [3].

Compared with traditional carbon materials, spherical carbon materials have unique advantages such as high density, high strength, smooth surface, unique spherical shape and high surface area. At present, it has been widely used as electrodes, absorbents, catalyst carriers, electrochemical protectors, super capacitors and so on [4,5].

The main fabricating methods of carbon spheres (CSs) include hydrothermal process, chemical vapor deposition (CVD), template method and high-temperature pyrolysis. CVD mainly uses gaseous

materials to fabricate fundamental particles. Various hydrocarbons have been used for fabricating CSs [6]. The predominant disadvantage of CVD is difficult to operate with high cost. Templates can be divided into soft template and hard template. The soft template is usually referring to surfactants which can confine the growth of CSs; the hard template is usually referring to rigid polymer spheres, alumina channels and mesoporous materials. Antonietti [7] fabricated nano-scale CSs by dipping sulfonated polystyrene spheres into metal salt solution. The main shortcoming of the template method is the complex reaction steps. Pyrolysis at high temperatures is another common method to fabricate CSs. Pol [8] fabricated uniform-sized CSs through high temperature pyrolysis. Reduction [9] and ultrasonic [10] are also reported to fabricate CSs.

However, hydrothermal synthesis is the most popular way to fabricate CSs. For the past few years, various organics have been used as raw materials to fabricate CSs at hydrothermal conduction, such as glucose, sucrose and plant fibers [11,12]. Wang [11] fabricated hard charcoals with good spherical morphology with the diameter of 0.4 nm. The specific surface area is about  $400\text{m}^2\text{g}^{-1}$  and its lithium storage capacity can reach  $430\text{mAhg}^{-1}$ . Mi [12] prepared CSs from glucose with high yields and narrow diameter distributions.

Even though the precursor-derived CSs is a good choice for electrodes, the poor hydrophilicity limits its applications due to the large resistance at the interfaces. Nitrogen doping is widely studied to modify the carbonaceous materials. It has been reported that certain nitrogen doping could improve capacitance [13,14], surface wettability [15], and electronic conductivity [16] while maintaining the super cyclic performance [17]. Furthermore, the electrodes doped with nitrogen can produce pseudo-capacitance behaviors [18] so that it may increase the specific capacitance of the carbon materials.

With the purpose to obtain excellent carbon-based super capacitors, we are trying to find an effective method to prepare N-doped CSs. Hydrothermal method is firstly considered and graphitic carbon nitride ( $\text{g-C}_3\text{N}_4$ ) quantum dots were chosen as the nitrogen source.  $\text{g-C}_3\text{N}_4$  is a melon polymer which can be easily obtained from the polycondensation of melamine, cyanamide, dicyandiamide, or urea [19]. Tri-s-triazine is generally recognized as the building block of  $\text{g-C}_3\text{N}_4$ . So pyridinic (N-6) and pyrrolic or pyridone (N-5) nitrogen can be easily introduced from  $\text{g-C}_3\text{N}_4$ . Herein we report the hydrothermal synthesis of N-doped CSs from glucose using polymeric  $\text{g-C}_3\text{N}_4$  quantum dots as the nitrogen source. Nitrogen are successfully introduced into the CSs and conductivity and specific capacitance are both improved. As a typical performance, the specific capacitance of the N-doped sample is as high as  $281\text{F/g}$  at  $2\text{A/g}$  in KOH electrolyte, which is 50 % higher than the performance of the un-doped sample.

## 2. EXPERIMENTAL

### 2.1. Synthesis of $\text{g-C}_3\text{N}_4$ quantum dots

Bulk  $\text{g-C}_3\text{N}_4$  was first synthesized from melamine (Analytical pure, Sinopharm Group Chemical Reagent Co., Ltd.). 10 g of melamine was heated to  $550\text{ }^\circ\text{C}$  with a rate of  $10\text{ }^\circ\text{C/min}$  and maintained at this temperature for 2 h. The  $\text{g-C}_3\text{N}_4$  dots were obtained by hydrothermal cutting of bulk

g-C<sub>3</sub>N<sub>4</sub> in water. In detail, 0.2 g of g-C<sub>3</sub>N<sub>4</sub> was dispersed in 60 mL water, transferred into a Teflon-sealed autoclave and maintained at 180 °C for 10 h [20]. The obtained suspension was then centrifuged with a rate of 10000 r/min to remove precipitates. The products were dispersed in water for further use. The final yield of the g-C<sub>3</sub>N<sub>4</sub> dots was approximately 26.5 %.

## 2.2. Synthesis of activated carbon spheres (ACSs)

The N-doped CSs were hydrothermal synthesized from a mixture of 45 ml (1 mol/L) glucose (Analytical pure, Sinopharm Group Chemical Reagent Co., Ltd.) and different masses of g-C<sub>3</sub>N<sub>4</sub> dots. The mixture was placed into a 100 mL Teflon-lined stainless steel autoclave, and then heated in an oven at 180 °C for 10 h. The obtained brown solid powder was filtered and washed with distilled water and methanol until the solution is neutral. Afterwards, the powder was dried in an oven at 60 °C for 12 h. Finally, the brown powder was carbonized at 800 °C under N<sub>2</sub> flow for 2 h to obtain a black N-doped carbon powders. The N-doped ACSs were eventually obtained after heating the black powders in air at 450 °C for 90 min. According to the mass ratio of g-C<sub>3</sub>N<sub>4</sub> dots, the ACSs were named as ACS-0, ACS-1, ACS-2, ACS-3, in which the introduced mass of g-C<sub>3</sub>N<sub>4</sub> dots is 0.0 g, 0.1 g, 0.2 g and 0.3 g respectively.

## 2.3. Characterization methods

The microstructures of the ACSs were investigated using the Quanta FEG 250 scanning electron microscope (SEM). Nitrogen adsorption-desorption isotherms were carried out using the BELSORP-mini II analyzer. The specific surface areas were calculated through BET method, and the pore size distributions were analyzed through BJH method. The Raman spectra were obtained using a laser confocal Raman spectrometer (BRUK-SENTERPA, 532 nm, 20 mW) in the range from 400 to 2000 cm<sup>-1</sup>. The crystalline structure was investigated using the D8ADVANCE X-ray diffraction (XRD, CuK-Alpha radiation,  $\lambda = 0.154$  nm), with  $2\theta$  from 10° to 90°. The atomic ratios were investigated using the K-Alpha 1063 type X-ray photoelectron spectroscopy (XPS) with focused monochromatized AlK-Alpha radiation (1486.6 eV).

## 2.4. Electrochemical performances

The electrodes were fabricated by mixing 80 wt% ACSs with 10 wt% acetylene black, 10 wt% N-methyl-2-pyrrolidone (NMP) solution of polyvinylidene fluoride. Afterwards, the mixed slurries were pasted on a stainless slice with an area mass density of 2 mg/cm<sup>2</sup>. These electrodes were then dried at 60 °C for 24 h in an oven. Electrochemical performances were carried out using an electrochemical working station equipped with a three-electrode system (CHI660a Electrochemistry Workstation, ShangHai Chen Hua Instrument Co. Ltd.). A Pt plate was used as the counter electrode, Hg/HgO as the reference electrode and the ACSs as the working electrode. 6 mol/L KOH aqueous solution was used as the electrolyte. Cyclic voltammetry (CV) was conducted from -1 to 0 V at different sweep rates ranging from 2 to 20 mV/s. Galvanostatic charge/discharge (GC) cyclic performance was recorded in the same voltage range at different current densities ranging from 2 to 10

A/g. The specific gravimetric capacitances were calculated on the basis of discharge profiles. Electrochemical impedance spectroscopy (EIS) was performed at open circuit voltages, with the variation of frequency ranging from 0.01 to 10KHz. The following formula [21] was used for calculating the specific capacitance.

$$C_{\text{spec}} = \frac{i\Delta t}{m\Delta v} \quad (1)$$

Where,  $C_{\text{spec}}$  is the specific capacitance of the capacitor (F/g),  $i$  is the discharge current (mA),  $\Delta t$  is the discharge time (s),  $m$  is the mass of the ACSs on the electrode and  $\Delta v$  is 1 V.

### 3. RESULTS AND DISCUSSION

#### 3.1. Morphologies and microstructures

Fig.1 shows SEM images of the ACSs. There are numerous micro-scale particles in perfect spherical morphology. Some holes can be observed on the surfaces, which are formed due to the decomposition of g-C<sub>3</sub>N<sub>4</sub> dots and the air-activations at high temperatures. The average diameter of N-doped samples are ~5.0  $\mu\text{m}$ , while the un-doped sample is only ~0.4  $\mu\text{m}$ . So g-C<sub>3</sub>N<sub>4</sub> dots play an important role in enlarging the ACSs.

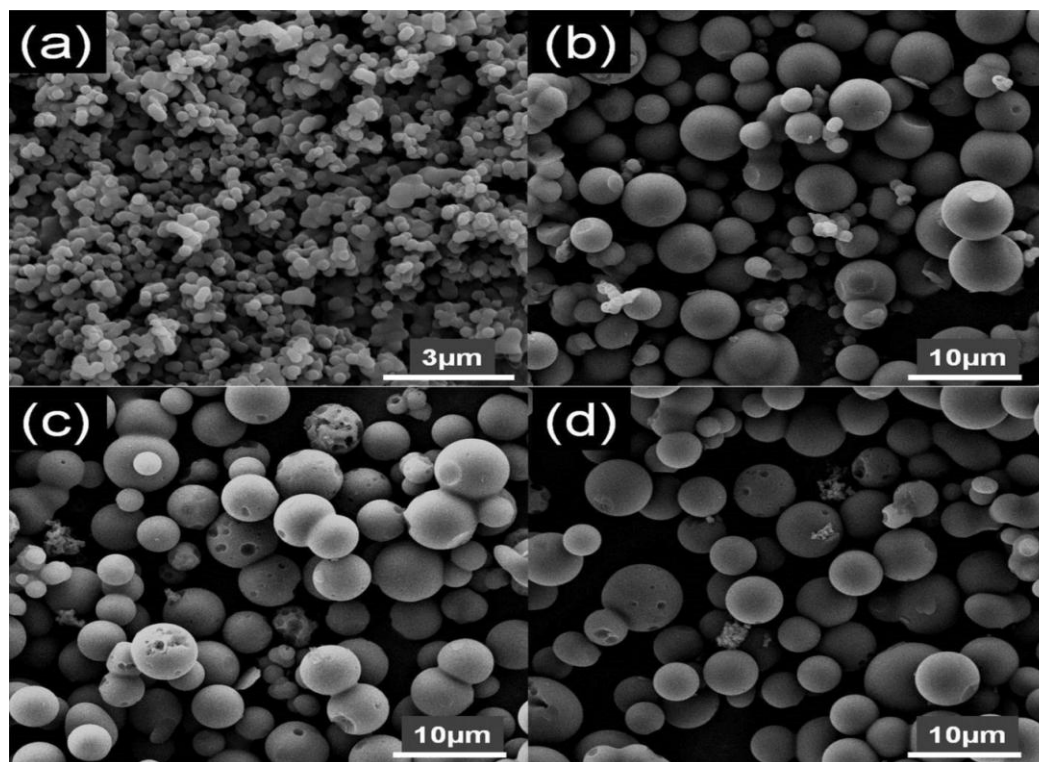


**Figure 1.** SEM images of the ACSs. (a)ACS-0, (b)ACS-1, (c)ACS-2 and (d) ACS-3.

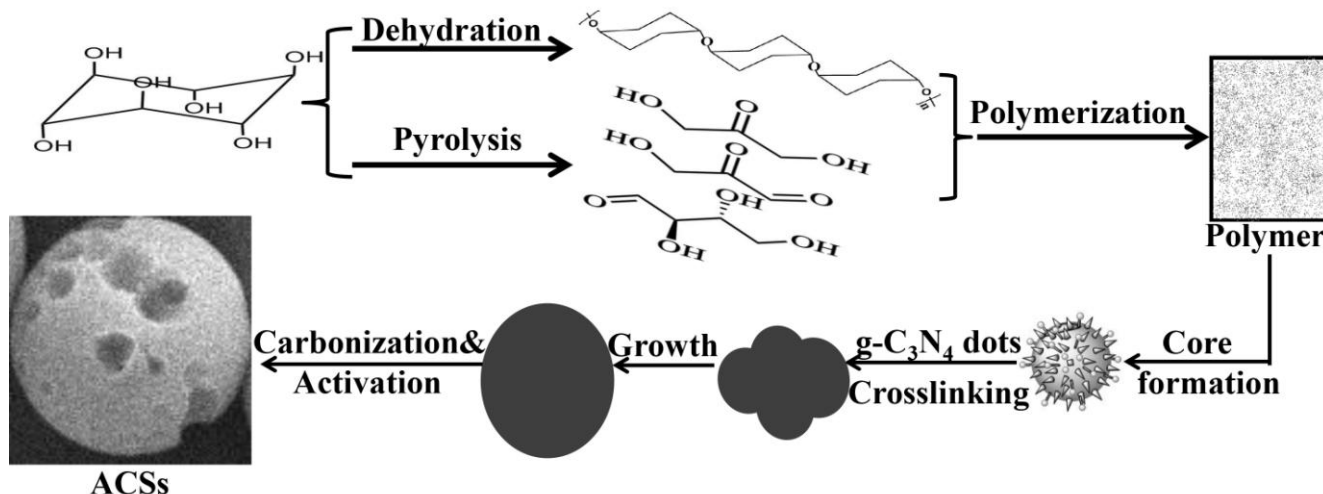


Figure 2. Formation mechanism of the ACSs.

Sun [22] found that the hydrothermal synthesis of microspheres behaves the Lamer model. Inspired by this model, the formation mechanism of the enlarged ACSs is illustrated in Fig.2. Firstly, under hydrothermal conditions, the glucose monomer transforms not only into ketones, aldehydes, and aromatic acids but also polymerizes into oligosaccharides. The carbonized core is formed through intermolecular dehydration or branched oligosaccharides. The resulting nuclei then grew uniformly and isotropically when the solutes diffuses toward the surfaces of the particles. g-C<sub>3</sub>N<sub>4</sub> dots act as cross-linking agent during the growth process. So finally an enlarged micro-scale ACS was obtained after the carbonization and activation process.

Table 1. Porous microstructures and disorder degrees of the ACSs.

Sample	S <sub>BET</sub> (m <sup>2</sup> /g)	V <sub>micro</sub> (cm <sup>3</sup> /g)	V <sub>meso</sub> (cm <sup>3</sup> /g)	d (nm)	I <sub>D</sub> /I <sub>G</sub>
ACS-0	1092	0.361	0.042	3.151	1.87
ACS-1	992	0.407	0.054	3.124	1.39
ACS-2	1048	0.370	0.034	3.101	1.43
ACS-3	1073	0.392	0.039	3.295	1.45

BET analysis was performed for the ACSs and is shown in Fig.3. According to the classification of the adsorption-desorption isothermal curves, the isothermal curves of the ACSs belong to the type-I curve with predominate micro-pores. The pore size distributions of the samples are shown in Fig.3b and the parameters derived wherefrom are shown in Table 1. The specific surface area of the ACSs are about 1000 m<sup>2</sup>/g, no remarkable change before and after the N-doping. The mesopore volume are much lower than the micropore volume, and the average pore diameter is ~3 nm. As shown in Table 1, ACS-1 has both the largest micropore volume and mesopore volume. The micropores are responsible for the capacitive charge by providing sufficient electrolyte ion adsorbing sites, while the mesopores generally facilitate ion mobility into micropores [23,24]. So among all the ACSs, ACS-1 has the greatest potential for electrode applications.

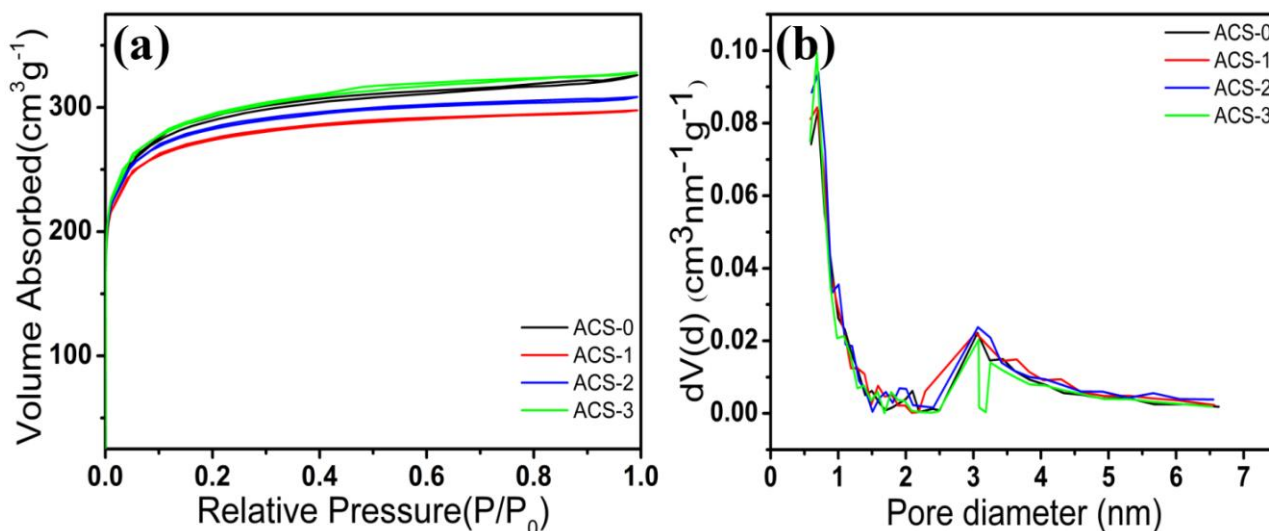


**Figure 3.** BET analysis of the ACSs. (a) Adsorption-desorption isothermal curves. (b) Pore size distributions.

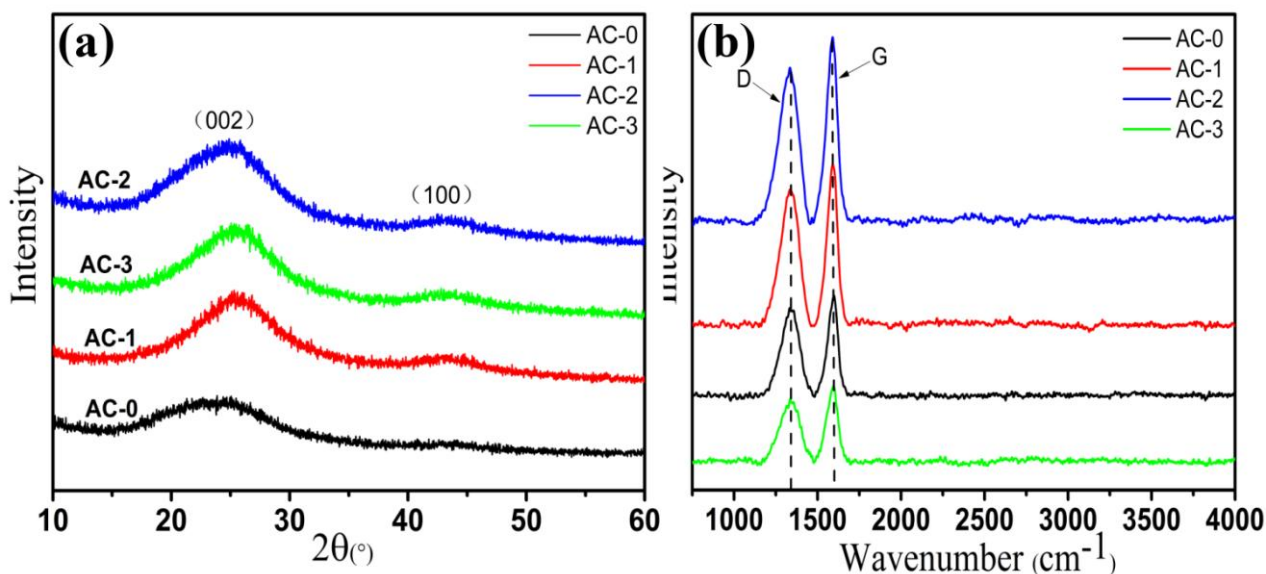


**Figure 4.** Crystallization behaviors of the ACSs. (a) XRD patterns. (b) Raman spectra.

XRD and Raman spectra of the ACSs are shown in Fig. 4. In Fig.4(a), there are two broad diffraction peaks at 26 ° and 43 °, corresponding to (002) and (100) graphic planes [25,26] respectively, indicating an amorphous state of the carbon materials [27]. The amorphous structure makes the electrolyte easy to penetrate into the electrode material, thereby increasing the utilization of the electrode material [28]. Raman spectra in Fig.4 (b) exhibit two main characteristic peaks of carbon materials, the G band (around 1582 cm<sup>-1</sup>) and the D band (around 1348 cm<sup>-1</sup>) [25,26]. The former peak is related to the well-ordered graphite crystallites, while the latter peak represents the disorders or defects in carbon microstructures. Generally, the values of  $I_D/I_G$  represent disorder degree of the materials, which is shown in Table 1. The higher of the disorder degree, the higher the ratio will be.

The values of  $I_D/I_G$  of the N-doped samples are all smaller than that of the un-doped sample, indicating a more ordered microstructure with the addition of g- $C_3N_4$  dots [29], even though all the ACSs are still in an amorphous state. The relatively higher order degree of the N-doped samples could enhance the electron conductivity and therefore improve the electrochemical performance.

### 3.2. Elemental contents and bonding states

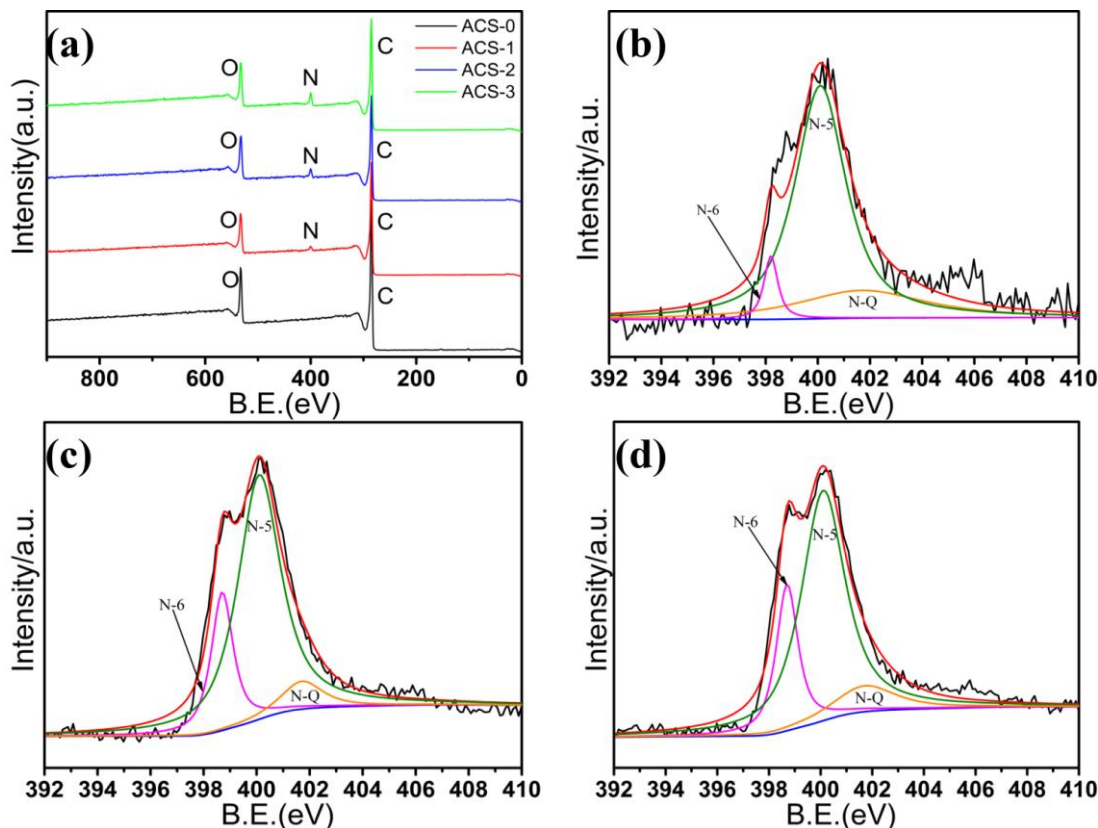


**Figure 5.** XPS analysis of the ACSs. (a) Full survey spectra. Deconvoluted N1s spectra of (b) ACS-1, (c) ACS-2 and (d) ACS-3.

X-ray photoelectron spectroscopy (XPS) was performed to study the specific nitrogen functionalities. The full survey spectra of all of the samples are shown in Fig.5(a) and the elemental contents calculated from the peaks are listed in Table 2. Nitrogen contents of the doped samples are increased from 2.56 to 6.48 at% with increase of the g- $C_3N_4$  dots from ACS-1 to ACS-3. The deconvolutions of the N1s peaks are shown in Fig.5 (b-d) and fitted with three individual peaks, which can be attributed to three types of nitrogen groups, namely pyrrolic/pyridone (N-5), pyridinic (N-6), and quaternary nitrogen (N-Q). As reported [30,31], the introduced nitrogen elements in the carbon matrix could not only bring pseudo capacitance to the material, but also enhance surface wettability maximizing surface area utilizations. In this work, nitrogen is introduced in the forms of N-5 and N-6 and the amount of N-6 is increasing with the increase of the nitrogen content. So g- $C_3N_4$  dots is an efficient nitrogen source for introducing N-5 and N-6 into carbonaceous materials.

**Table 2.** Elemental contents and specific capacitances of the ACSs.

Sample	C (at%)	N (at%)	O (at%)	$n_{N-5}/n_{N-6}$	$C_{spec}$ (F/g)
ACS-0	85.68	0.0	14.32	-	182
ACS-1	83.64	2.56	13.80	13.47	281
ACS-2	80.12	4.20	15.67	9.09	193
ACS-3	78.81	6.48	14.71	6.27	241

### 3.3. Electrochemical properties

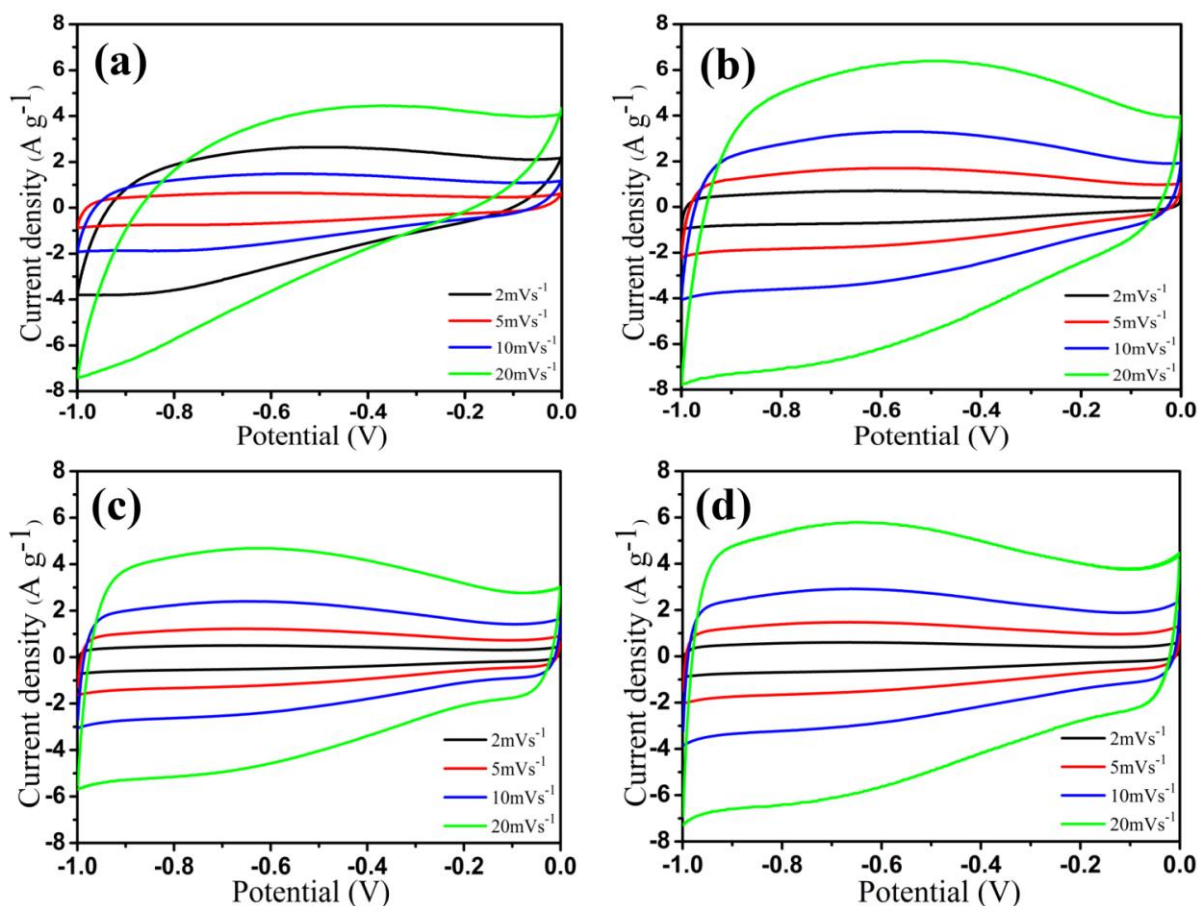
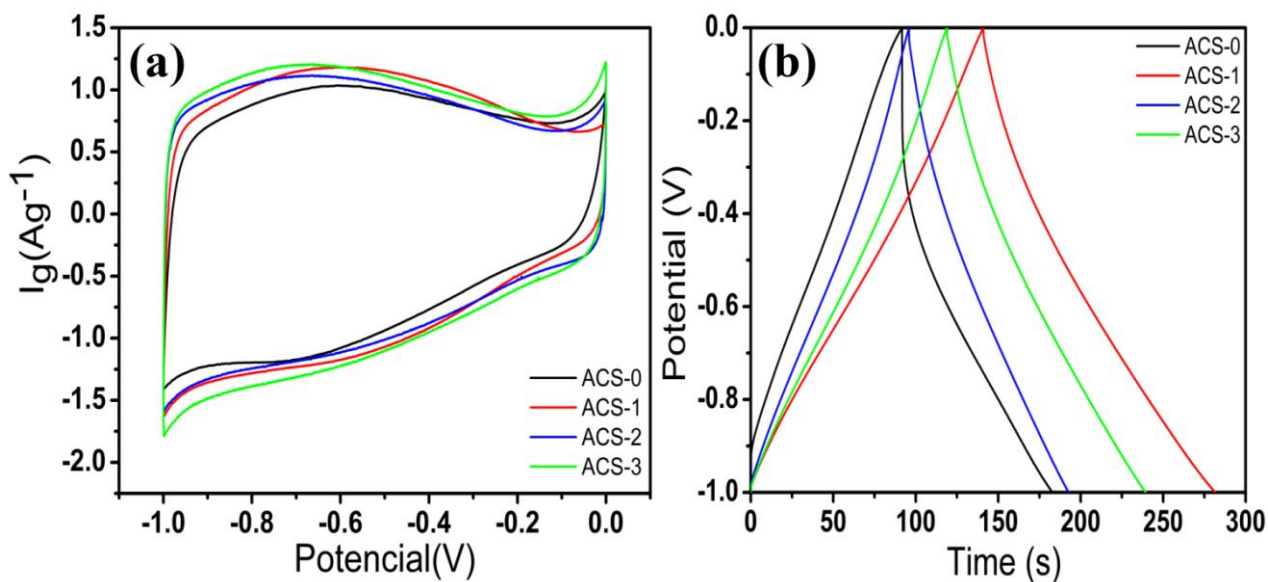
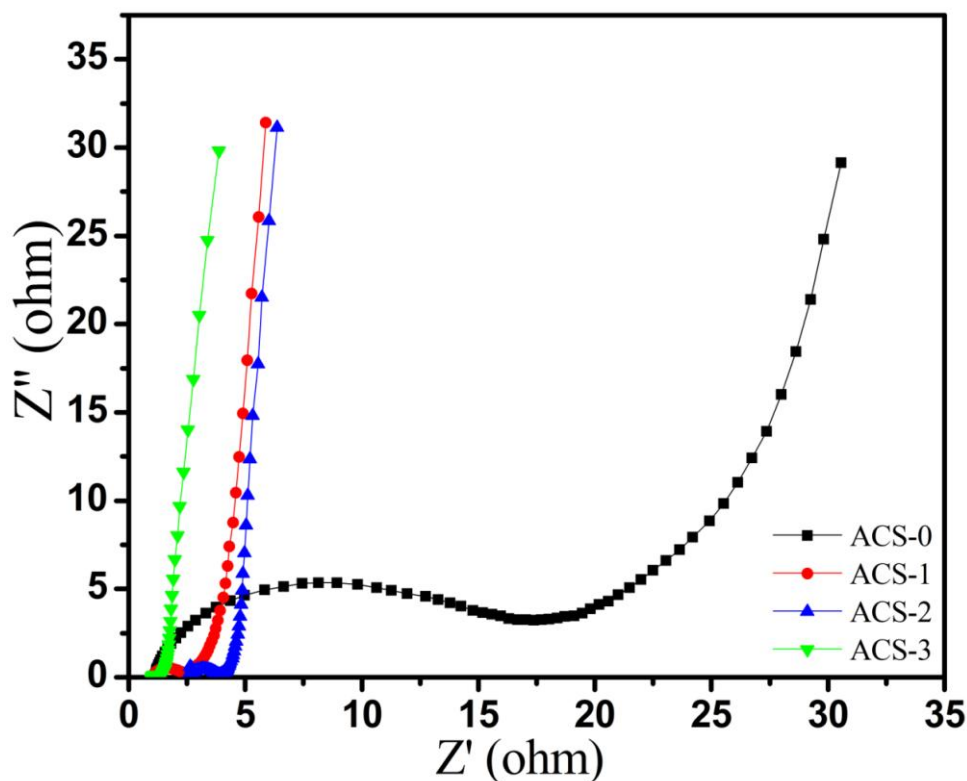
**Figure 6.** Cyclic voltammetric curves at different scan rates. (a)ACS-0, (b)ACS-1, (c)ACS-2 and (d) ACS-3.

Fig.6 shows the cyclic voltammetric (CV) curves of the ACSs at different scan rates. The curve of the un-doped sample exhibits significant distortions from 2 to 20 mV/s, as shown in Fig. 6(a). Comparatively, as shown in Fig.6(b-d), the curves of the N-doped samples maintain a consistent appearance from 2 to 20 mV/s. It indicates that the N-doped samples have much increased double layer capacities, with much improved rate capability and reversibility.



**Figure 7.** Performance comparison of the ACSs. (a) Cyclic voltammetric curves at 2 mV/s and (b) charge and discharge curves at 2 A/g.



**Figure 8.** Impedance spectra of the ACSs.

The CV curves at 2 mV/s are extracted and comparatively shown in Fig.7(a). The rectangular CV curves of the N-doped samples have a relatively larger area than the un-doped samples. This is contributed by the nitrogen groups that make the electrolyte ions having sufficient time to enter the pores of the materials [32,33]. The voltage drop of the N-doped samples are lower than the un-doped

sample. In general, small voltage drop indicates low internal resistance and excellent capacitive behaviors. The charge and discharge curves shown in Fig.7(b) exhibit nearly symmetrical triangles. In addition, the N-doped samples exhibit longer charge/discharge time than the un-doped sample, demonstrating significantly enhanced capacitive performance, which is in agreement with the CV measurements. The calculated specific capacitances are listed in Table 2, showing a much improved specific capacitance from 182 F/g to 281 F/g with 2.56 at% nitrogen doping.

Impedance spectra of the ACSs were conducted and are shown in Fig. 8. The intercept at Z'axis is related to the total internal resistances ( $R_s$ ) [34,35]. It shows that all the N-doped samples have much lower  $R_s$  than the un-doped samples. The low  $R_s$  is beneficial for high power applications. The semicircle at high frequency represents the charge transfer resistance ( $R_{ct}$ ). Generally, a smaller semicircle means a lower  $R_{ct}$  [33,36]. As shown in Fig.8, the N-doped samples exhibit decreased  $R_{ct}$  compared to the un-doped sample. The projected lengths on Z'axis for the N-doped samples are all shorter than the un-doped sample, indicating enhanced ion diffusion rate into the interior pores of the electrodes, accounting for more effective utilization of the surface area [33,37].

#### 4. CONCLUSIONS

N-doped activated carbon microspheres, approximately 5  $\mu\text{m}$  in diameter, were obtained using a simple hydrothermal treatment of glucose and g- $\text{C}_3\text{N}_4$  dots. g- $\text{C}_3\text{N}_4$  dots are capable of introducing pyridinic (N-6) and pyrrolic/pyridone (N-5) into the carbonaceous materials. Cyclic voltammetry curves, charge-discharge curves and impedance curves confirm that the N-doped samples have much improved double-layer capacitance storage and charge-discharge rate. The specific capacitance of the N-doped sample is as high as 281 F/g at 2 A/g, which is 50 % higher than the performance of the un-doped sample. So this work demonstrates that g- $\text{C}_3\text{N}_4$  dot is a good additive agent for nitrogen doping and thus the enhancement of the electrochemical properties.

#### ACKNOWLEDGEMENTS

T. Yan and J. Xu contributed equally to the work. The whole work was carried out at National University of Defense Technology (NUDT) through a Master Joint Supervision System.

#### References

1. D. Kalpana, S.H. Cho, S.B. Lee, Y.S. Lee, R. Misra and N.G. Renganathan, *J. Power Sources*, 190 (2009) 587.
2. K. Kierzek, E. Frackowiak, G. Lota, G. Gryglewicz and J. Machnikowski, *Electrochim. Acta*, 49 (2004) 515.
3. K. Zheng, X. Fan, Y. Mao, J. Lin, W. Dai, J. Zhang and J. Cheng, *Sci. Rep.*, 6 (2016) 20306.
4. L. Yang, H. Li, H.Z. Liu and Y.Y. Zhang, *Int. J. Electrochem. Sci.*, 12 (2017) 1.
5. A.A. Deshmukh, S.D. Mhlanga and N.J. Coville, *Mater. Sci. Eng. R*, 70 (2010) 1.
6. Y.Z. Jin, C. Gao, W.K. Hsu, Y. Zhu, A. Huczko, M. Bystrzejewski, M. Roe, C.Y. Lee, S. Acquah, H. Kroto and D.R.M. Walton, *Carbon*, 43 (2005) 1944.

7. M. Antonietti, F. Gröhn, J. Hartmann and L. Bronstein, *Angew. Chem. Int. Ed.*, 36 (1997) 2080.
8. V.G. Pol, M. Motiei, A. Gedanken, J. Calderon-Moreno and M. Yoshimura, *Carbon*, 42 (2004) 111.
9. G. Hu, D. Ma, M. Cheng, L. Liu and X. Bao, *Chem. Commun.*, 8(2002) 1948.
10. Z. Wang, L. Yu, W. Zhang, Z. Zhu, G. He, Y. Chen and G. Hu, *Phys. Lett. A*, 307 (2003) 249.
11. Q. Wang, H. Li, L. Chen and X. Huang, *Carbon*, 39 (2001) 2211.
12. Y. Mi, W. Hu, Y. Dan and Y. Liu, *Mater. Lett.*, 62 (2008) 1194.
13. D. Hulicova-Jurcakova, M. Seredych, G.Q. Lu and T.J. Bandosz, *Adv. Funct. Mater.*, 19 (2009) 438.
14. H.M. Jeong, J.W. Lee, W.H. Shin, Y.J. Choi, H.J. Shin, J.K. Kang and J.W. Choi, *Nano Lett.*, 11 (2011) 2472.
15. H. Guo and Q. Gao, *J. Power Sources*, 186 (2009) 551.
16. Y.H. Lee, Y.F. Lee, K.H. Chang, and C.C. Hu, *Electrochem. Commun.*, 13 (2011) 50.
17. H.J. Denisa, K. Masaya, S. Soshi, H. Hiroaki, Z.H. Zhu and G.Q. Lu, *Adv. Funct. Mater.*, 19 (2009) 1800.
18. E. Frackowiak, *Phys. Chem. Chem. Phys.*, 9 (2007) 1774.
19. B. Yuan, X.S. Zou, T.N. Yan, J.J. Fei and Z.Y. Chu, *J. Nanopart. Res.*, 18(2016) 110.
20. S. Zhang, J. Li, M. Zeng, J. Xu, X. Wang and W. Hu, *Nanoscale*, 6 (2014) 4157.
21. S. Ding, T. Zhu, J. S. Chen, Z. Wang, C. Yuan and X.W. Lou, *J. Mater. Chem.*, 21 (2011) 6602.
22. X. Sun and Y. Li, *Angew. Chem. Int. Ed.*, 43 (2004) 597.
23. M. Zhi, F. Yang, F. Meng, M. Li, A. Manivannan and N. Wu, *ACS Sustain. Chem. Eng.*, 2 (2014) 1592.
24. P. Kleszyk, P. Ratajczak, P. Skowron, J. Jagiello, Q. Abbas, E. Frackowiak and F. Béguin, *Carbon*, 81 (2015) 148.
25. V. Jiménez, P. Sánchez, J. L. Valverde and A. Romero, *J. Colloid Interface Sci.*, 336 (2009) 712.
26. Y.J. Hwang, S.K. Jeong, K.S. Nahm, J.S. Shin and A.M. Stephan, *J. Phys. Chem. Solids*, 68 (2007) 182.
27. R. Xue and Z. Shen, *Carbon*, 41 (2003) 1862.
28. E. Mora, C. Blanco, J. A. Pajares, R. Santamaría and R. Menéndez, *J Colloid Interface Sci.*, 298 (2006) 341.
29. L. Chen, Z. Wang, C. He, N. Zhao, C. Shi, E. Liu and J. Li, *ACS Appl. Mater. Interfaces*, 5 (2013) 9537.
30. W. Li, D. Chen, Z. Li, Y. Shi, Y. Wan, J. Huang, J. Yang, D. Zhao and Z. Jiang, *Electrochem. Commun.*, 9 (2007) 569.
31. T.E. Rufford, D. Hulicova-Jurcakova, E. Fiset, Z. Zhu and G.Q. Lu, *Electrochem. Commun.*, 11 (2009) 974.
32. Z. Jin, W. Mu, C. Zhang, T. He, Q. Zhang, J. Hou and K. Cai, *Electrochim. Acta*, 59 (2012) 100.
33. A.G. Pandolfo and A.F. Hollenkamp, *J. Power Sources*, 157 (2006) 11.
34. Y. Shang, Z. Yu, C. Xie, Q. Xie, S. Wu, Y. Zhang and Y. Guan, *J. Solid State Chem.*, 19 (2015) 949.
35. J. Chang, Z. Gao, X. Wang, D. Wu, F. Xu, X. Wang, Y. Guo and K. Jiang, *Electrochim. Acta*, 157 (2015) 290.
36. T.C. Girija and M.V. Sangaranarayanan, *J. Power Sources*, 156 (2006) 705.
37. Q. Xie, R. Bao, A. Zheng, Y. Zhang, S. Wu, C. Xie and P. Zhao, *ACS Sustain. Chem. Eng.*, 4 (2016) 1422.